Experiments on cold-formed ferritic stainless steel slender sections

Bock M, Arrayago I and Real E

Department of Construction Engineering, Universitat Politècnica de Catalunya, UPC

C/ Jordi Girona, 1-3. 08034 Barcelona, Spain

* Corresponding author: Tel: +0034 934054156, Fax: +0034 934054135, e-mail: marina.bock@upc.edu

Abstract

The usage of stainless steel in construction has been increasing owing to its corrosion resistance, aesthetic appearance and favourable mechanical properties. The most common stainless steel grades used for structural applications are austenitic steels. The main drawback of these grades relies on their nickel content (around 8-10%), resulting in a relatively high initial material cost. Other stainless steel grades with lower nickel content such as the ferritic steels offer the benefits of stainless steels in terms of functional qualities and design but within a limited cost frame. Hence, ferritic stainless steels may be a viable alternative for structural applications. Given the fact that little experimental information on ferritic stainless steels is currently available, the purpose of this investigation is to report a series of material and cross-section tests on ferritic grade EN 1.4003 (similar to 3Cr12) stainless steel square and rectangular hollow sections to enable a better understanding of their material response and structural performance. Four different cross-section geometries have been tested under pure compression and in-plane bending. Measurements of geometric imperfections and material properties are also presented. The obtained test results are used to assess the adequacy of the slenderness limits and effective width formula given in EN 1993-1-4 to ferritic stainless steels, those proposed by Gardner and Theofanous and Zhou et al. design approach.

Highlights

- Experimental study of ferritic stainless steel stub columns and beams
- Local buckling of cross-sections with different aspect ratios
- Applicability of various design methods for cross-section design to ferritic stainless steel
- Design recommendations

Keywords

Effective width, element interaction, experiments, ferritic stainless steel, slenderness limits, local buckling

1. Introduction

The chromium present within the internal crystalline structure of stainless steels forms a self-healing passivation layer of chromium oxide (Cr_2O_3) when exposed to oxygen preventing surface corrosion. Other alloying elements are added to meet specific needs in terms of strength, corrosion resistance and ease of fabrication. Depending on their chemical composition, stainless steels can be classified into main five categories: ferritic, austenitic, martensitic, duplex and precipitation hardening. The most commonly used materials in construction are the austenitic grades which have reasonable mechanical strength with 0.2% proof stress of 210-240 N/mm^2 and display high ductility with ultimate strains ε_u laying between 50 and 60%. These positive features, however, may be inhibited by the high initial material cost and considerable price fluctuations associated with the amount of nickel involved in austenitic stainless steels (8-11%). Ferritic stainless steels, on the other hand, contain little nickel leaving chromium as the main alloying element (min. 10.5%); hence, they are price stable and cheaper alloys. In comparison with the austenitic grades, the initial material cost of ferritic stainless steels is about three times lower which makes them an attractive alternative for structural applications. Despite their low nickel content, which may reduce ductility and increase risk of pitting corrosion, ferritic stainless steels offer a good combination of mechanical and corrosion-resistance properties with higher 0.2% proof stress of 250-330 N/mm^2 in the annealed condition and they are easier to work and machine in comparison with the austenitics. Moreover, by increasing the chromium content (10.5-30%) and including establishing alloying elements such as molybdenum and niobium, similar corrosion resistance to some austenitics grades can be achieved without compromising the initial material cost.

The viability of ferritic stainless steels for structural applications has been recently investigated within the framework of a RFCS European project [2] where the applicability of various aspects of the European design guidance for stainless steels, EN 1993-1-4 [1], to this material was examined. The specifications for cross-section design given in EN 1993-1-4 [1], have been assessed for application to ferritic stainless steel on the basis of experimental data [3-5] and generated numerical models within the context of that European project [6]. However, a fully experimental validation is yet required especially for cross-sections comprising slender elements. Hence, the purpose of this paper is to describe a comprehensive laboratory testing program on grade 1.4003 stainless steel slender tubular sections featuring square and rectangular hollow sections (SHS and RHS, respectively) conducted at the Universitat Politècnica de Catalunya. A total of 8 stub column tests and 9 beam tests, including 3-point bending and 4-point bending configurations were carried out. The mechanical material properties were determined at Acerinox Europa S.A.U where 16 tensile coupon tests, including both flat and corner specimens, were performed. The obtained test results have been used to assess the applicability of the slenderness limits and the accuracy of the effective width equations for slender elements given in EN 1993-1-4 [1]. The revised slenderness limits and effective width formula proposed by Gardner and Theofanous [7] as well as the design approach derived by Zhou et al. [8] have also been considered herein. Relevant conclusions regarding various appraisals are presented and design recommendations are proposed.

2. Experimental investigation

2.1 Introduction

An experimental investigation including 8 stub column tests and 9 beam tests was performed on ferritic stainless steel SHS and RHS in the Laboratori de Tecnologia d'Estructures Luis Agulló, in the Department of Construction Engineering at Universitat Politècnica de

Catalunya. Four section sizes were examined (h×b×t): SHS 60×60×2, RHS 70×50×2, RHS 80×40×2 and RHS 100×40×2, see Fig. 1. The investigated sections provided height to width ratios of 1, 1.4, 2 and 2.5. The specimens were cold-rolled from annealed flat strips of 1.4003 stainless steel and were delivered by the manufacturer in appropriate lengths to perform material and structural tests. The chemical composition and the tensile properties of the coil material used to form the various specimens are given in Table 1 and Table 2, respectively, as provided by the steelmaker in the mill certificates.

Table 1. Chemical composition of grade EN 1.4003 stainless steel from mill certificates

Section	C %	Si %	Mn %	P %	S %	Cr %	Ni %	N %	CO %
SHS 60×60×2	0.012	0.250	1.440	0.029	0.002	11.300	0.400	0.016	0.010
RHS 70×50×2	0.012	0.290	1.440	0.030	0.001	11.200	0.400	0.009	0.010
RHS 80×40×2	0.012	0.280	1.400	0.030	0.001	11.400	0.400	0.010	0.010
RHS 100×40×2	0.015	0.370	1.480	0.027	0.002	11.200	0.400	0.009	0.010

Table 2. Mechanical properties from mill certificates

Section	$\sigma_{0.2}$ (MPa)	$\sigma_{1.0}$ (MPa)	σ_u (MPa)	ε_f
SHS 60×60×2-T1	355	379	491	0.41
SHS 60×60×2-T2	342	363	479	0.40
RHS 70×50×2-T1	349	371	496	0.38
RHS 70×50×2-T2	350	368	484	0.40
RHS 80×40×2-T1	353	377	501	0.38
RHS 80×40×2-T2	351	372	496	0.37
RHS 100×40×2-T1	373	408	529	0.23
RHS 100×40×2-T2	350	379	498	0.24

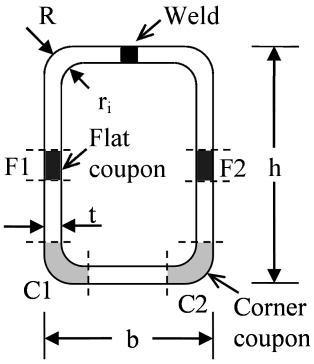

Fig. 1 Definition of symbols and location of coupon in cross-section

2.2 Material tests

A series of tensile coupon tests were conducted at Acerinox Europa S.A.U to determine the basic stress-strain response of the ferritic stainless steel specimens. All the tested coupons were extracted from the batch of the specimens selected for the tests. Two tensile flat coupons were taken from two faces of the SHS and RHS specimens in the longitudinal direction, resulting in a total of 8 tensile coupon tests. All tensile flat coupons were machined into parallel necked specimens with a standard gauge length of $5.65\sqrt{A_c}$, where A_c is the cross-sectional area of the coupon, and width of 15 mm. Additional corner coupons were extracted from the curved portions of each of the cross-sections extended two times the thickness through the flat region in order to quantify the corner strength enhancements induced by the cold-forming process [9, 10]. A total of 16 material tests were performed.

Having extracted both flat and corner coupon tests, a longitudinal curving of all coupon specimens was observed. This was due to the release of the through-thickness bending residual stresses induced during the manufacturing process and present in the final cross-section. All the coupons almost returned to their flat state during gripping in the testing machine's jaws [11, 12]. Hence, the obtained stress-strain responses inherently include the effect of longitudinal through-thickness bending residual stresses. Membrane residual stresses were not explicitly measured since previous studies [13,14] concluded that their effect is relatively small compared to bending residual stresses.

The coupons were placed in a hydraulic machine (see Fig. 2 (a)) and were tested according to [15]. The test were conducted at uniform strain rate of 0.00025 s^{-1} up to the 0.2% proof stress and then increased up to 0.008 s^{-1} until fracture. A data acquisition system was employed to record load and displacement at regular intervals while testing by using a data logger piece of software. Typical tensile coupon fractures are presented in Fig. 2 (b) and 2 (c) for the flat and the corner coupons, respectively.

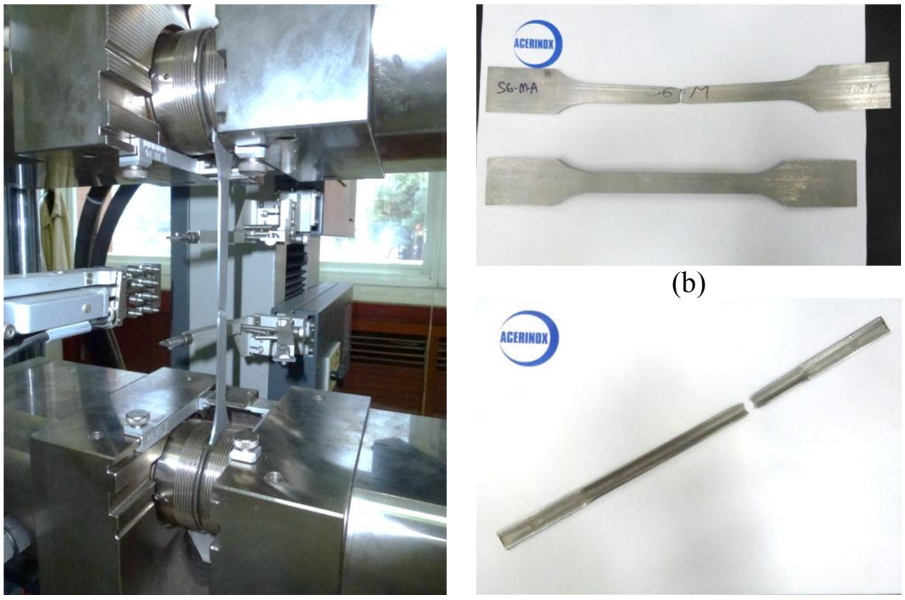

(a) (b) (c)

Fig. 2 Material test hydraulic machine (a) and typical coupon fractures in (b) flat coupons and (c) corner coupons

The material properties obtained from the coupon tests are summarized in Table 3 where the coupons have been labelled beginning with the section geometry e.g. SHS 60×60×2, followed by the coupon type, F for tensile flat, C for tensile corner, and finally the section face number (1, 2), as given in Fig. 1. The material parameters reported in Table 3 are the Young's modulus E, the dynamic 0.01%, 0.05% and 0.2% proof stresses $\sigma_{0.01}$, $\sigma_{0.05}$ and $\sigma_{0.2}$ respectively, and the maximum achieved ultimate tensile stress σ_u with its corresponding ultimate strain ε_u. These material property values can be used to replicate the whole stress-strain curve on the basis of the compound Ramberg-Osgood material models available in the literature [16-19]. The weighted average material properties based on face width and corner properties extended two times the thickness through the flat region of each section are given in Table 4. Typical stress-strain response of tensile flat and tensile corner ferritic stainless steel material are depicted in Fig. 3.

Table 3. Material properties for the tensile coupons

Coupon	E (Gpa)	$\sigma_{0.01}$ (MPa)	$\sigma_{0.05}$ (MPa)	$\sigma_{0.2}$ (MPa)	σ_u (MPa)	ε_u
60×60×2-F1	173	331	396	437	484	0.108
60×60×2-F2	161	324	382	425	473	0.114
70×50×2-F1	178	323	378	418	479	0.137
70×50×2-F2	175	325	381	419	480	0.138
80×40×2-F1	182	321	379	416	484	0.138
80×40×2-F2	172	330	383	419	486	0.147
100×40×2-F1	181	332	382	416	481	0.134
100×40×2-F2	174	334	385	416	484	0.132
60×60×2-C1	172	361	475	552	571	0.008
60×60×2-C2	163	360	468	544	564	0.009
70×50×2-C1	180	394	489	556	576	0.011
70×50×2-C2	178	370	479	554	573	0.012
80×40×2-C1	184	364	456	552	580	0.010
80×40×2-C2	177	396	492	592	611	0.006
100×40×2-C1	182	378	482	558	578	0.012
100×40×2-C2	177	363	445	548	580	0.008

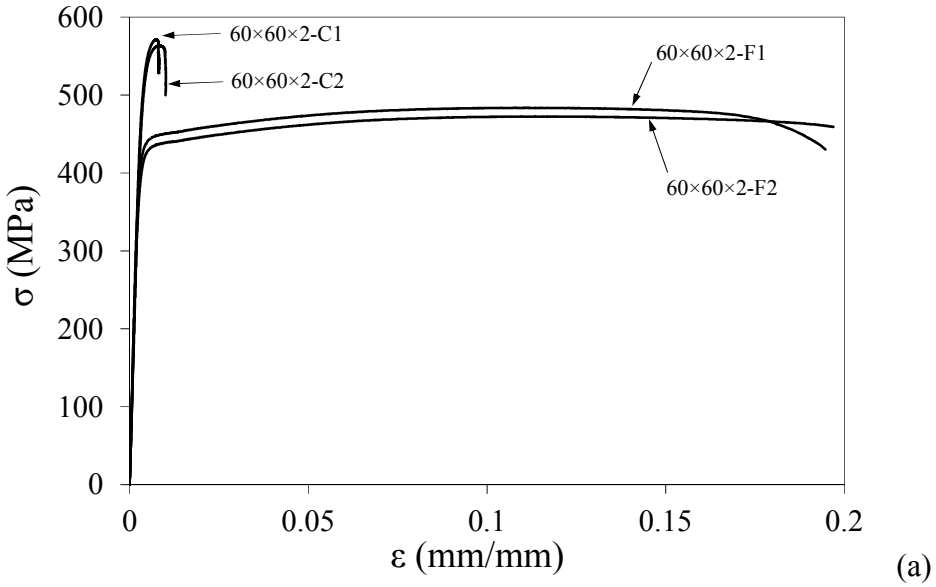

(a)

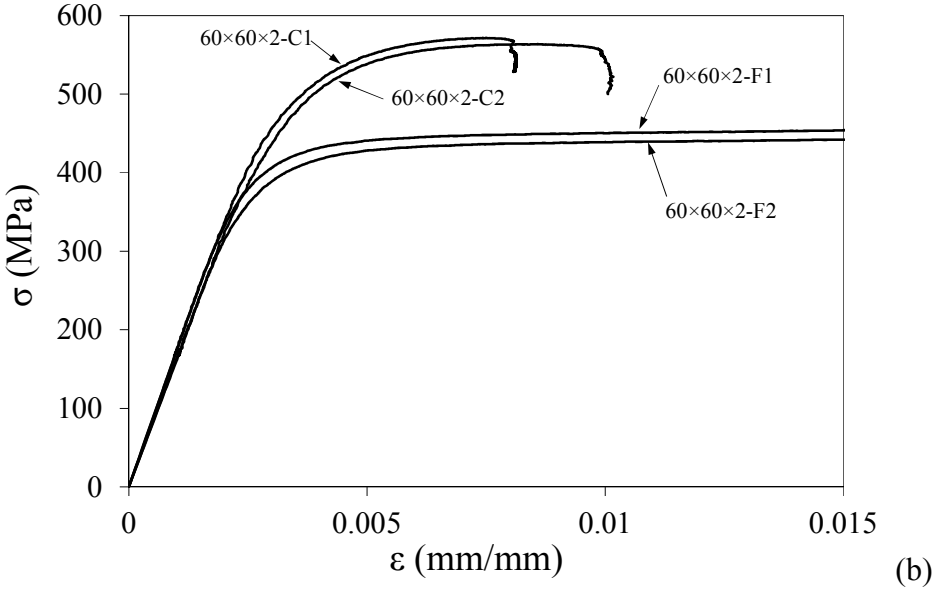

(b)

Fig. 3 (a) Full stress-strain curves for flat tensile and corner tensile material taken from SHS 60×60×2 and (b) detail of the material nonlinearity

Table 4. Weighted average tensile material properties

Section	E (Gpa)	$\sigma_{0.01}$ (MPa)	$\sigma_{0.05}$ (MPa)	$\sigma_{0.2}$ (MPa)	σ_u (MPa)	ε_u
SHS 60×60×2	167	335	409	459	499	0.086
RHS 70×50×2	176	337	404	450	502	0.108
RHS 80×40×2	177	338	400	451	508	0.113
RHS 100×40×2	178	341	399	443	501	0.109

2.3 Stub Column tests

Two repeated concentric stub column tests were performed on four ferritic stainless steel slender cross-sections: SHS 60×60×2, RHS 70×50×2, RHS 80×40×2 and RHS 100×40×2. All the specimens were selected to be short enough to avoid global flexural buckling but with enough length to include a representative pattern of residual stresses and geometric imperfections according to [20]. Hence, stub column lengths were equal to three times the largest nominal cross-sectional dimension. Prior to testing, measurements of each cross-section dimensions and initial geometric imperfections were conducted, which were measured at the location 180º (opposite face) and 90º angles from the weld. A linear variable differential transformer (LVDT) was used to obtain readings along the middle half of these faces of each specimen. The data was collected by passing the specimen, which was placed on a table of a milling machine, under the LVDT via an automatic feed at a fixed rate of 30 cm per minute. All the data was recorded at 2 s^{-1} intervals using the data acquisition system MGCplus and logged using the Catman Easy computer package. The obtained imperfection spectrums exhibited the expected half sine wave. The maximum measured imperfection from both faces was then averaged to determine the imperfection magnitude w_0 given in Table 5. This table also reports the measured geometry (see Fig. 1) of each stub column specimen where L is the stub column length, h is the section depth, b is the section width, t is the thickness, r_i is the internal corner radius and A is the area of the cross-section.

Table 5. Measured dimensions of the stub column specimens and imperfection magnitudes

Specimen	L (mm)	h (mm)	b (mm)	t (mm)	r_i (mm)	A (mm^2)	w_0 (mm)
60×60×2-SC1	179.5	60.3	60.3	2.00	2.4	454	0.02
60×60×2-SC2	180.0	60.3	60.4	2.02	2.3	460	0.02
70×50×2-SC1	210.0	70.1	49.9	2.00	2.3	451	0.03
70×50×2-SC2	210.0	70.0	49.8	1.99	2.2	450	0.03
80×40×2-SC1	240.0	80.0	40.5	2.00	1.3	457	0.06
80×40×2-SC2	240.0	80.0	40.3	1.99	1.9	453	0.06
100×40×2-SC1	299.5	100.1	40.0	2.05	2.1	546	0.07
100×40×2-SC2	299.5	100.1	40.5	1.99	2.2	532	0.07

The specimens were tested in compression between parallel flat platens in an Instron 1000kN hydraulic testing machine as shown in Fig. 4. The test was driven by displacement control at 0.5 mm/min. The instrumentation consisted of three LVDTs to measure the end shortening between both flat platens, a load cell to accurately record the compressive load and two strain gauges affixed at the mid-height of the largest plate width of the cross-section and at a distance two times the material thickness from mid-width of the face. The strain readings, which were taken from the first set of tests (SC1), were used to verify the concentricity of the loading distribution and to remove the elastic deformation of the flat platens. All the data, including load, displacement, voltage and strain were recorded at 2 s^{-1} intervals using the data acquisition system MGCplus and logged using the Catman Easy computer package.

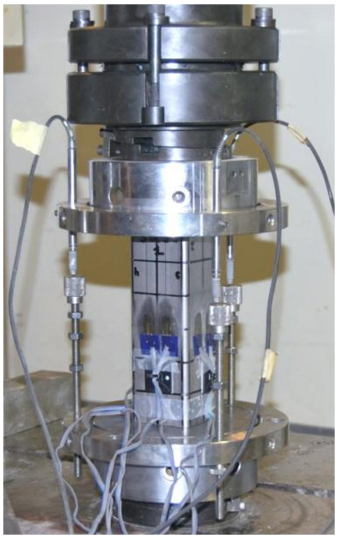

Fig. 4 Stub column test setup – Specimen 60×60×2-SC1

The experimental ultimate loads $N_{u,test}$ of the test specimens and their corresponding end shortenings δ_u are given in Table 6. The full end-shortening response for all the specimens is shown in Fig. 5 on a normalised basis by the plastic resistance of the gross cross-section N_{pl}. Note that the similarity between the first (SC1) and the repeated test (SC2) for all the tested sections demonstrates the reliability of the test results. The reported end-shortening measurements given in Table 6 and Fig. 5 refer to the true stub column shortening δ. In determining this value, the elastic deformation of the end platens was eliminated following the guidelines of [21] and as given by Eq. (1) where δ_{LVDT} is the LVDT end shortening and δ_{platen} is the end platen deformation given in Eq. (2) where L is the length of the stub column specimen, σ is the applied stress, and $E_{0,LVDT}$ and $E_{0,true}$ are Young's moduli of the LVDTs and strain gauge response, respectively. All the specimens failed by local buckling and typical failure modes are shown in Fig. 6.

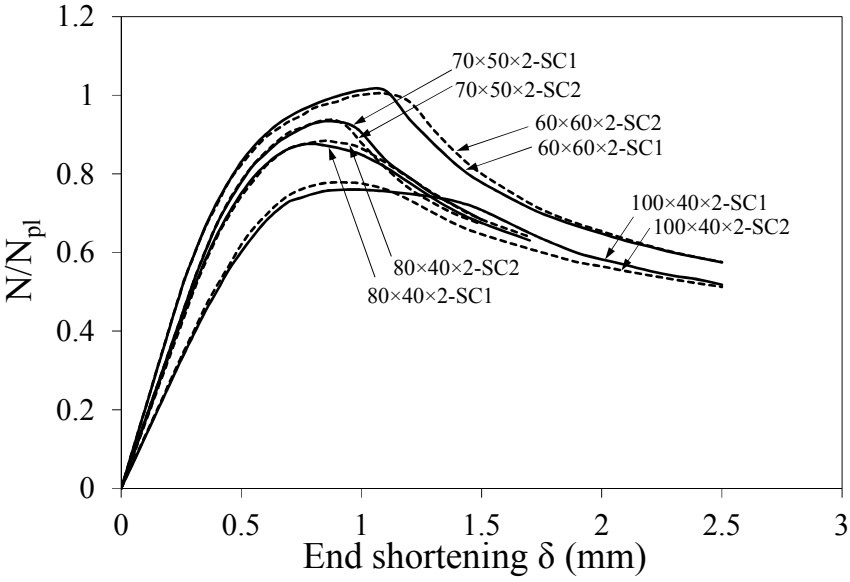

Fig. 5 Load-end shortening response for the tested stub columns

Table 6. Summary of the results for the stub columns

Specimen	$N_{u,test}$ (kN)	End shortening at ultimate load δ_u (mm)
60×60×2-SC1	211.37	1.02
60×60×2-SC2	212.31	1.03
70×50×2-SC1	190.15	0.87
70×50×2-SC2	190.05	0.84
80×40×2-SC1	178.21	0.80
80×40×2-SC2	179.52	0.82
100×40×2-SC1	184.23	0.97
100×40×2-SC2	183.99	0.92

$$\delta = \delta_{LVDT} - 2\delta_{platen} \tag{1}$$

$$\delta_{platen} = \frac{L}{2}\sigma\left(\frac{1}{E_{0,LVDT}} - \frac{1}{E_{0,true}}\right) \tag{2}$$

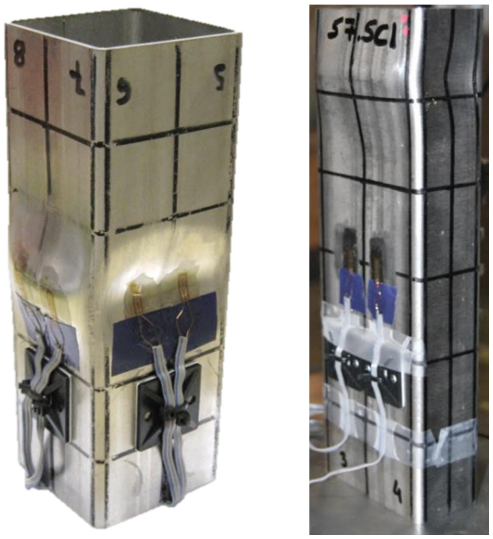

(a) (b)

Fig. 6 Stub column failure modes: Specimens (a) 60×60×2-SC1 and (b) 80×40×2-SC1

2.4 Beam tests

A total of 9 in-plane bending tests, including 3-point (3P) and 4-point (4P) load configurations were conducted to determine the flexural response of ferritic stainless steel SHS and RHS. All four sections SHS 60×60×2, RHS 70×50×2, RHS 80×40×2 and RHS 100×40×2 were tested under 4-point bending configuration about both major (Mj) and minor (Mi) axis while sections SHS 60×60×2 and RHS 80×40×2 were tested under 3-point bending configuration about minor axis. All the beams were simply supported with spans of 1500 mm and extended 100 mm beyond the simple supports at each end resulting in a total length of 1700 mm. The supports, which were steel rollers, allowed axial displacement of the beam. Although the tubular geometry of the specimens precluded lateral torsional buckling, possible lateral displacement was prevented placing stabilizers at both supports in contact with the beam through teflon plates provided with a layer of grease to minimize friction and allow in-plane rotation.

Prior to testing, measurements of each cross-section dimensions and initial geometric imperfections were taken following the same procedure conducted in section 2.2 for the stub column specimens. The measured geometry and imperfection magnitudes w_0 of each beam are reported in Table 7 where W_{el} and W_{pl} are the elastic and the plastic section modulus, respectively.

Table 7. Measured dimensions of the beam specimens and imperfection magnitudes

Specimen	Axis of bending	L (mm)	H (mm)	B (mm)	t (mm)	r_i (mm)	W_{el} (mm^3)	W_{pl} (mm^3)	w_0 (mm)
60×60×2-3P	-	1700.0	60.1	60.1	2.10	2.2	8741	10233	0.02
80×40×2-3P	Minor	1700.0	80.0	40.3	2.08	2.0	6621	7483	0.06
60×60×2-4P	-	1700.0	60.1	60.1	2.05	2.5	8532	9983	0.02
70×50×2-4P	Major	1700.0	70.1	49.8	1.93	2.4	8625	10358	0.03
70×50×2-4P	Minor	1700.0	70.1	49.9	2.03	2.2	7548	8638	0.03
80×40×2-4P	Major	1699.5	80.0	40.5	2.02	2.4	9422	11712	0.06
80×40×2-4P	Minor	1699.0	79.9	40.3	2.08	2.1	6598	7458	0.06
100×40×2-4P	Major	1699.5	100.1	40.0	2.05	1.9	13400	16967	0.07
100×40×2-4P	Minor	1699.5	100.1	39.9	2.05	2.0	7931	8846	0.07

The tested beams were loaded symmetrically in a 1000 kN hydraulic testing machine at mid-span for the 3-point configuration while for the 4-point bending tests, the load was applied at two points (510 mm from each support) as shown in Figs 7 and 8, respectively. Load cells were placed under both supports to verify symmetry of loading while testing. Position sensors (Temposonic) were located at loading points to measure vertical deflections in both test arrangements while a string potentiometer was additionally placed at mid-span for the 4-point bending tests. In order to determine the end rotation of the beams, two inclinometers were positioned at each end of the beams. Strain gauges were affixed at the top and bottom flanges of the beams at 60 mm from the mid-span for the 3-point bending tests and at mid-span for the 4-point bending tests. Specimen RHS 80×40×2-3P tested about minor axis under 3-point bending configuration was monitored with four strain gauges at both top flange and web to recode the onset of local buckling as well as material and post-buckling nonlinear effects. Wooden blocks were placed within the tubes and were carefully located under the loading points to prevent web crippling failure for the 4-point configuration and the specimen 80×40×2-3P-Mi tested about minor axis under the 3-point configuration. The load was applied through elastomeric bearing plates and the test was driven by displacement control at a rate of 3 mm/min. All the data, including load, displacement, voltage and strain was recorded at 2 s^{-1} intervals using the data acquisition system MGCplus and logged using the Catman Easy computer package.

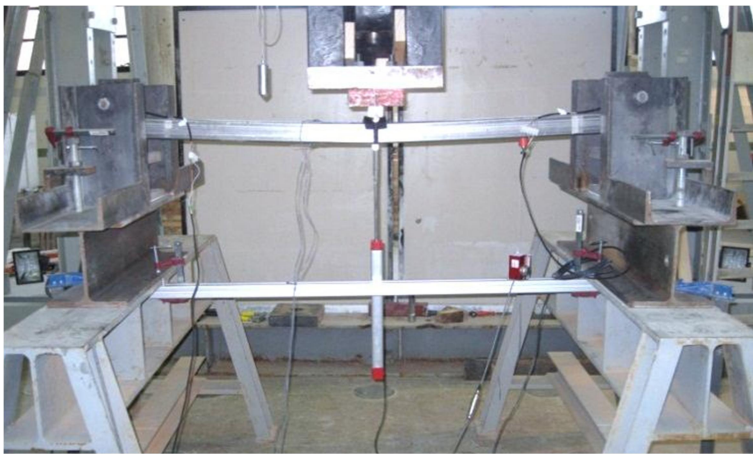

Fig. 7 Test arrangement for the 3-point bending test (3P) – Specimen 60×60×2-3P

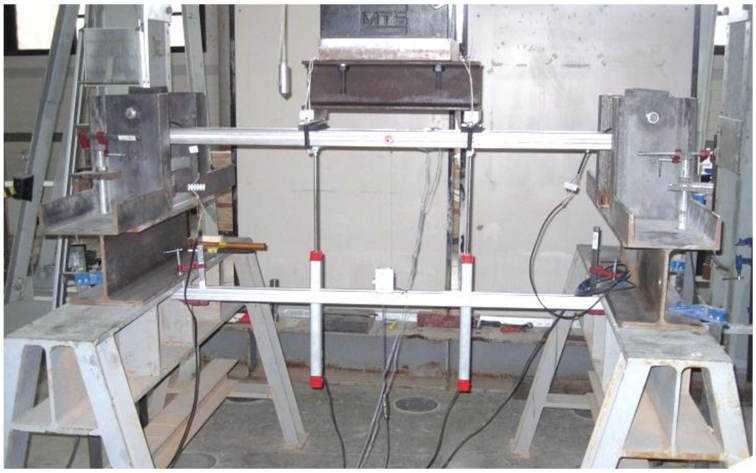

Fig. 8 Test arrangement for the 4-point bending test (4P) – Specimen 80×40×2-4P-Mi

The experimental ultimate bending moment $M_{u,test}$, together with other key experimental results are presented in Table 8. Recall that specimen 60×60×2-3P was not provided with wooden blocks and consequently, web crippling and bending interaction effects were observed in the test result. In determining the corrected value for the ultimate bending moment given in Table 8, the effective moment resistance of the cross-section determined deducting the ineffective areas according to the reduction factor ρ given in EN 1993-1-4 [1] and the interaction bending moment and local load equation given in EN 1993-1-3 [22] was used. Full moment-rotation and moment-curvature curves from the 3-point bending tests and the 4-point bending tests are presented in Figs 9 and 10, respectively, where θ is the mid-span rotation determined as the sum of the measurements taken by the two inclinometers and κ is the curvature calculated according to [23] and as given by Eq. (3) where u_{ms} is the deflection at mid-span measured by the string potentiometer, u_{av} is the average of the vertical displacement at loading points defined as $u_{av}=(u_1+u_2)/2$ and taken from the temposonic sensors measurements, and L is the distance between the loading points.

$$\kappa = \frac{8(u_{ms} - u_{av})}{4(u_{ms} - u_{av})^2 + L^2} \tag{3}$$

Table 8. Summary of test results for the beams

Specimen	Axis of bending	Ultimate moment $M_{u,test}$ (kNm)	θ_{pl} or κ_{pl}	R
60×60×2-3P	-	3.90*	8.04E-02	-
80×40×2-3P	Minor	2.87	1.08E-01	-
60×60×2-4P	-	4.22	1.07E-04	-
70×50×2-4P	Major	4.90	8.74E-05	1.90
70×50×2-4P	Minor	3.50	1.17E-04	-
80×40×2-4P	Major	5.60	7.97E-05	0.72
80×40×2-4P	Minor	2.76	1.44E-04	-
100×40×2-4P	Major	6.29	6.30E-05	-
100×40×2-4P	Minor	3.08	1.40E-04	-

*Corrected value

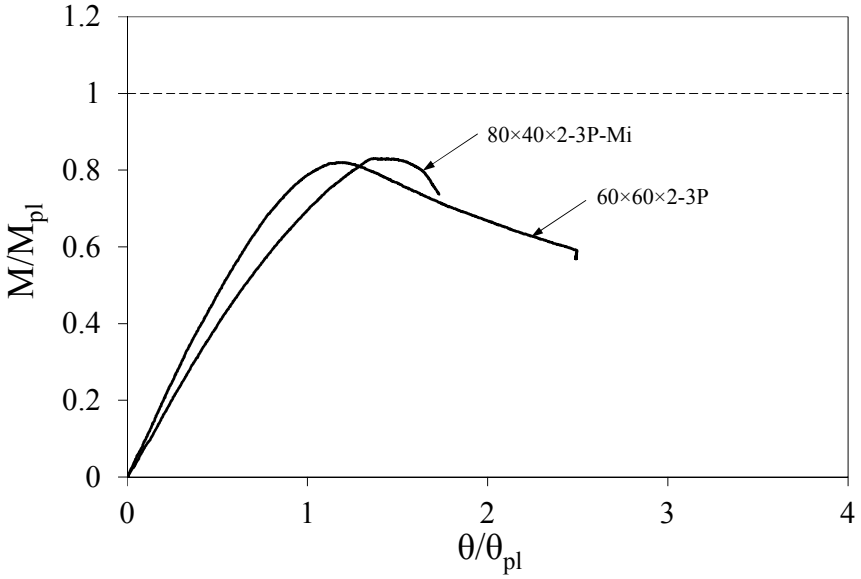

Fig. 9 Normalised moment-rotation curves for the three-point bending tests

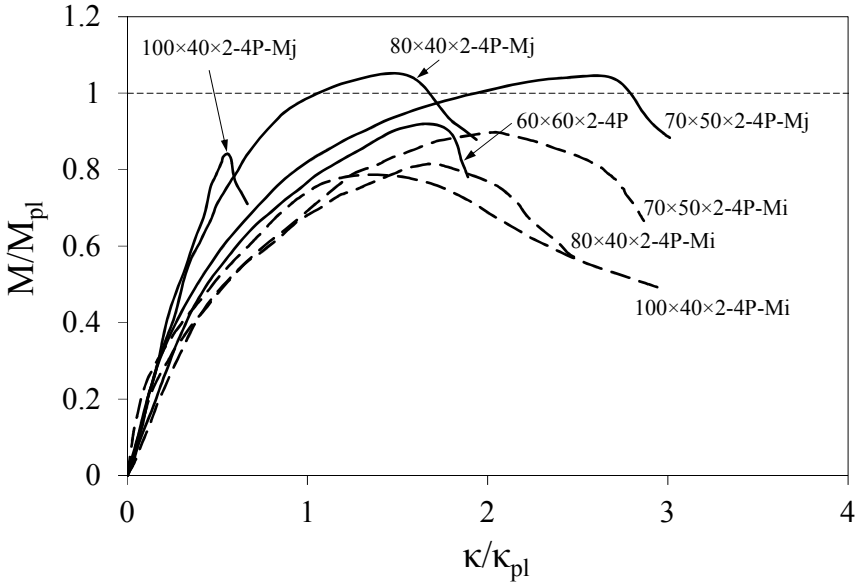

Fig. 10 Normalised moment-rotation curves for the four-point bending tests

The rotation capacity R reported in Table 8 was determined as $R=(\theta_u/\theta_{pl})-1$ and $R=(\kappa_u/\kappa_{pl})-1$ for the 3-point bending tests and the 4-point bending tests, respectively, where θ_u (κ_u) is the rotation (curvature) at which the moment-rotation (moment-curvature) curve falls below M_{pl} on the descending branch and θ_{pl} (κ_{pl}) is the elastic part of the total rotation (curvature) corresponding to M_{pl} in the ascending branch determined as $\theta_{pl}=M_{pl}L/2EI$ ($\kappa_{pl}=M_{pl}L/EI$), which is also given in Table 8, where I is the second moment of area of the section. Note that, given the slenderness nature of the cross-sections, most of the failures are achieved prior to the attainment of the plastic moment M_{pl} exhibiting no or little rotation capacity.

Typical local buckling modes were observed for all the specimens under both test arrangements as depicted in Fig. 11 (a) and 11 (b) for the 3-point bending and 4-point bending test configurations, respectively.

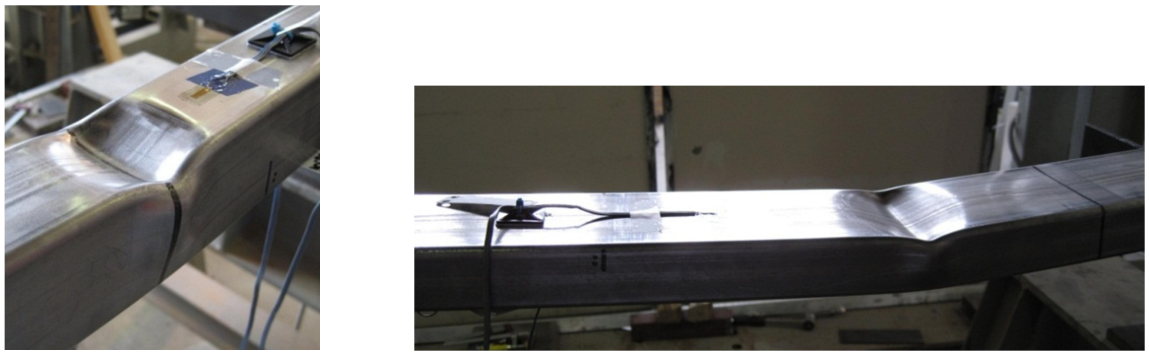

(a) (b)

Fig. 11 Typical (a) 3-point bending failure mode - Specimen 60×60×2-3P and (b) 4-point bending failure mode - Specimen 100×40×2-4P-Mi

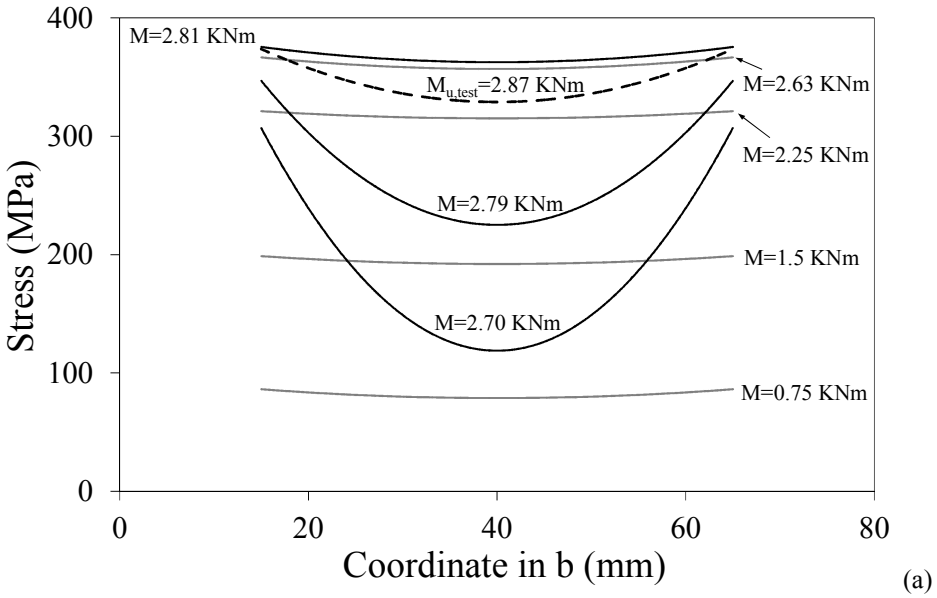

(a)

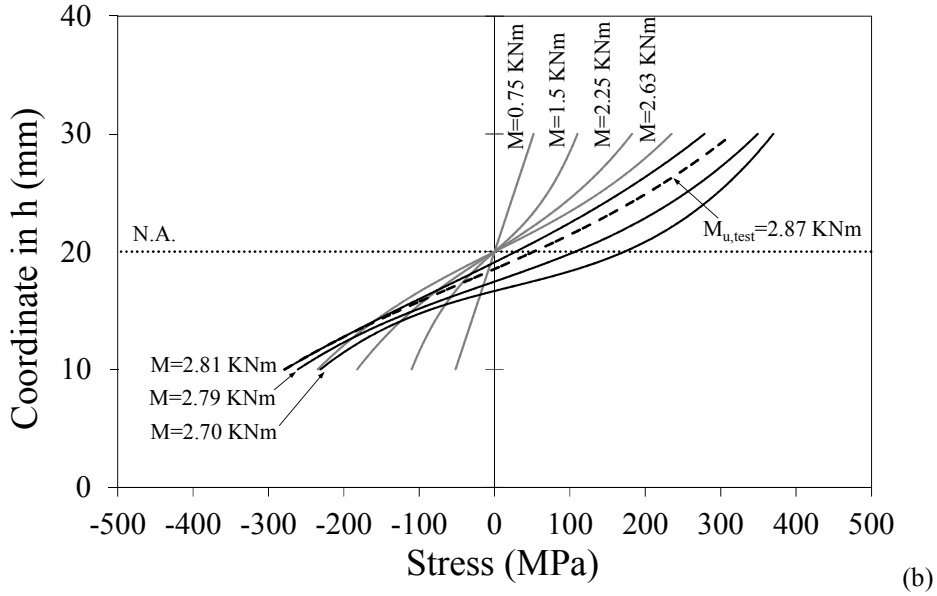

(b)

Fig. 12 Local buckling response in the specimen 80×40×2-3P-Mi

For the specimen 80×40×2-3P-Mi, which was monitored by affixing additional strain gauges as mentioned earlier, the evolution of the stresses along the compressed flange and the web under bending is presented in Fig. 12 (a) and 12 (b), respectively. For the former, strain measurements were taken at coordinates 15, 30, 50 and 65 mm along the cross-section width while for the latter the gauges were placed at 10, 16, 23 and 30 mm from the bottom flange. In these figures, a linear stress distribution is observed up to the onset of local buckling in the compressed flange, which is the most slender element, for an applied moment of M=2.81kNm. Beyond this point, the stresses in the compressed flange (Fig. 12 (a)) are transferred to the edge portion of the plate resulting in the typical non-uniform stress distribution pattern assumed by the effective width theory (post-buckling behaviour) for slender cross-sections. Consequently, the neutral axis (N.A.) of the web subjected to bending (Fig. 12 (b)) is shifted downwards. Note that the stress distribution in the web does not remain linear due to the actual non-linear material response exhibited by stainless steel.

3. Analysis of results and design recommendations

3.1 General

The European structural stainless steel design standard, EN 1993-1-4 [1], accounts for the effects of local buckling through the cross-section classification concept given in EN 1993-1-1 [24]. The procedure to classify a cross-section is based on the determination of the slenderness parameter $c/t\varepsilon$, where c is the flat width, t is the element thickness and ε is the material factor defined as $\varepsilon=[(235/\sigma_{0.2})(E/210000)]^{0.5}$. This parameter is then compared to different slenderness limits defining the different cross-sectional classes which depend on the manufacturing process (cold-formed or welded), the boundary conditions (internal or outstand elements) and the stress gradient (fully compressed, bending or combined compression and bending). In this procedure, all the constituent elements of the cross-section are assumed to be under simply supported conditions, hence neglecting the effect of element interaction. The whole cross-section classification relates to its most slender constituent element. Local buckling effects on slender cross-sections are accounted for by means of the effective width method applying a reduction factor ρ to the various plate widths that make up the cross-section so that the ineffective areas are deducted.

With the benefit of a far greater pool of experimental data than was available when EN 1993-1-4 [1] was published, Gardner and Theofanous [7] proposed new slenderness limits and revised the effective width formulae which have been experimentally verified for a variety of stainless steels and cross-sections [5,25-27] but still require further assessment, particularly for ferritic stainless steel slender sections. Slender sections are significantly influenced by the effects of element interaction, performing a higher structural response for higher aspect ratios $\alpha=h/b$ due to the degree of restraint provided by the flanges to the webs. Zhou et al. [8] derived a new design procedure to account for element interaction effects by proposing different Class 3 slenderness limits and reduction factor ρ equations for a given aspect ratio α. This approach was derived on the basis of generated numerical models on high strength stainless steel sections and its applicability to other grades might be examined.

The obtained experimental results on ferritic SHS and RHS stub column and beam tests are therefore used through this section to assess the slenderness limits and effective width formula used for cross-section design given in the current European specification for stainless steel, EN 1993-1-4 [1], those proposed by Gardner and Theofanous [7] as well as Zhou et al. [8] design approach to ferritic stainless steel. The assessment covers internal elements in compression and bending.

3.2 Assessment of Class 3 slenderness limit and cross-section resistance

3.2.1 Elements in compression

Both results from stub column and bending tests have been employed to assess the Class 3 slenderness limit for internal elements in compression. To this end, the relevant response $N_{u,test}/A\sigma_{0.2}$ or $M_{u,test}/W_{el}\sigma_{0.2}$, where A is the area of the gross cross-section, W_{el} is the elastic section modulus, $\sigma_{0.2}$ is the 0.2% proof stress based on the weighted average value given in Table 4 and $N_{u,test}$ and $M_{u,test}$ are the ultimate test load and moment, respectively, has been plotted against the slenderness parameter c/tε of the most slender constituent element controlling the local buckling response as shown in Figs 13 and 14 for the stub columns and the beams, respectively. The corresponding Class 3 limits given in EN 1993-1-4 [1], revised in [7] and proposed in [8] are also shown. Note that a cross-section is deemed to be Class 3 (or better) if $N_{u,test}$ (or $M_{u,test}$) exceeds $A\sigma_{0.2}$ (or $W_{el}\sigma_{0.2}$). In determining the most slender element in terms of the relevant slenderness $\overline{\lambda}_p$, simply supported conditions and appropriate stress distribution under which the flat elements of the cross-section are subjected were assumed to calculate the buckling factor k_σ as given by EN 1993-1-5 [28]. Table 9 shows the values of the relevant response together with the slenderness of the web $\overline{\lambda}_{p,w}$ and the flange $\overline{\lambda}_{p,f}$, and the slenderness parameter c/tε for the cross-sectional plate elements of all the specimens, where c_f and c_w are the flat portion of the flange and the web, respectively.

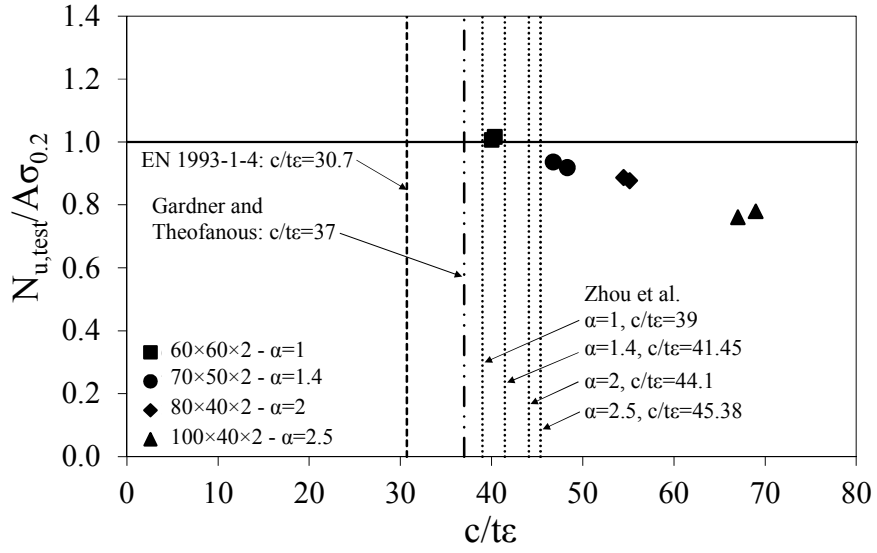

Fig. 13 Assessment of Class 3 limit for internal elements in compression (stub column test results)

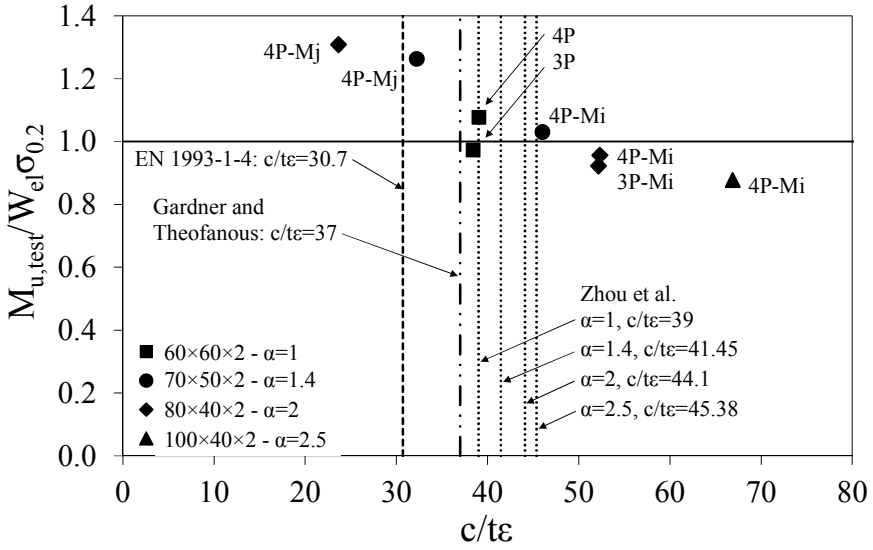

Fig. 14 Assessment of Class 3 limit for internal elements in compression (bending test results)

Table 9. Relevant response and slenderness parameters for all the specimens

Specimen	$c_w/t\varepsilon$	$c_f/t\varepsilon$	$\overline{\lambda}_{p,w}$	$\overline{\lambda}_{p,f}$	Controlling element	Stress distribution
60×60×2-SC1	39.97	40.01	0.70	0.70	Web/flange	Compressed
60×60×2-SC2	40.36	40.36	0.71	0.71	Web/flange	Compressed
60×60×2-3P	38.41	38.41	0.28	0.67	Flange	Compressed
60×60×2-4P	39.05	39.05	0.28	0.69	Flange	Compressed
70×50×2-SC1	48.30	32.47	0.85	0.57	Web	Compressed
70×50×2-SC2	46.76	31.45	0.82	0.55	Web	Compressed
70×50×2-4P-Mj	48.11	32.23	0.35	0.57	Flange	Compressed
70×50×2-4P-Mi	30.91	46.01	0.22	0.81	Flange	Compressed
80×40×2-SC1	55.14	25.49	0.97	0.45	Web	Compressed
80×40×2-SC2	54.49	24.49	0.96	0.43	Web	Compressed
80×40×2-3P-Mi	23.39	52.32	0.17	0.92	Flange	Compressed
80×40×2-4P-Mj	53.24	23.64	0.38	0.42	Flange	Compressed
80×40×2-4P-Mi	23.25	52.16	0.17	0.92	Falnge	Compressed
100×40×2-SC1	68.97	24.17	1.21	0.43	Web	Compressed
100×40×2-SC2	67.01	23.18	1.18	0.41	Web	Compressed
100×40×2-4P-Mj	67.13	23.36	0.48	0.41	Web	Bending
100×40×2-4P-Mi	23.08	66.88	0.17	1.18	Flange	Compressed

From Figs 13 and 14, it might be concluded that the current EN 1993-1-4 [1] Class 3 limit of 30.7 is appropriate for application to ferritic stainless steel, but conservative, while the revised slenderness value of 37 proposed by Gardner and Theofanous [7] better fits the test results. Zhou et al. [8] slenderness limiting values given in Eq. (4) provide good agreement with test data for an aspect ratio of α=1 (SHS) except for the specimen 60×60×2 tested under 3-point bending configuration which failed by bending and web crippling interaction. For aspect ratios α>1 (RHS) there are not enough representative data to draw a conclusion and further research is required to trace the trend of the structural response of the tested sections over the slenderness axis. However, the experimental results seem to achieve higher ultimate response with increasing aspect ratio and decreasing slenderness thereby reflecting the benefits of the element interaction effects and allowing less restrictive slenderness limits which is in line with the basis of Zhou et al. [8] design approach. It is therefore recommended

the Class 3 limit of 37 proposed by Gardner and Theofanous [7] for ferritic stainless steel cross-sections in light of the available resources which indicate the necessity to research on the effects of element interaction to extend Zhou et al. [8] proposal for application to ferritic steels.

$$\frac{c}{t\varepsilon} = \begin{cases} 30.5 + 10.2\alpha - 1.7\alpha^2 & 1 \le \alpha \le 3 \\ 45.8 & \alpha > 3 \end{cases} \quad \begin{matrix} \text{For } 488 \le \sigma_{0.2} \le 707 \text{ MPa} \\ \text{and } 1 \le \alpha \le 6 \end{matrix} \quad [8] \qquad (4)$$

Another aspect that should be mentioned in Figs 13 and 14 is that, ignoring the combined bending and web crippling interaction failure of specimen 60×60×2 tested under 3-point bending configuration, an assessment based on compression data leads to a stricter Class 3 limit [6, 29]. Thereby, the results from the stub column tests are used herein to assess the effective width formula for internal elements in compression used for cross-section design specified in EN 1993-1-4 [1] given in Eq. (5), and those proposed by Gardner and Theofanous [7] given in Eq. (6) and by Zhou et al. [8] given in Eqs (7) and (8). It is worth noting that the two former approaches apply the reduction factor ρ to the cross-sectional areas of the flat part of the elements of the cross-section classified as Class 4 while in the latter approach ρ is applied to the whole cross-section. Therefore, for the assessment of EN 1993-1-4 [1] and revised Gardner and Theofanous [7] proposal presented in Fig. 15, the reduction factor ρ determined as $\rho = \left(N_{u,num}/\sigma_{0.2} - A_r - 2 \cdot t \cdot c_f\right)/2 \cdot t \cdot c_w$ where $N_{u,test}$ is the ultimate load achieved in the tests, $\sigma_{0.2}$ is the 0.2% proof strength, A_r is the area of the corners, t is the thickness and c_f and c_w are the flat portion of the flange and the web respectively, has been plotted against the relevant slenderness $\overline{\lambda}_p$ of the most slender element, while for Zhou et al. approach the relevant response $N_{u,test}/A\sigma_{0.2}$ has been used in the vertical axis as shown in Fig. 16.

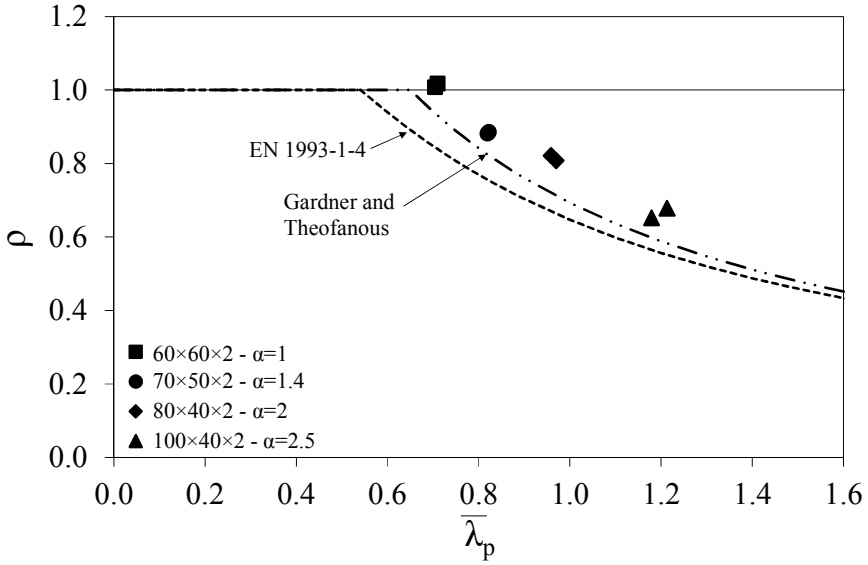

Fig. 15 Assessment of effective width formulae given in EN 1993-1-4 [1] and proposal in [7] for internal compressed elements

$$\rho = \frac{0.772}{\overline{\lambda}_p} - \frac{0.125}{\overline{\lambda}_p^2} \le 1 \text{ with } \overline{\lambda}_p \ge 0.541 \text{ [1]} \qquad (5)$$

$$\rho = \frac{0.772}{\overline{\lambda}_p} - \frac{0.079}{\overline{\lambda}_p^2} \le 1 \text{ with } \overline{\lambda}_p \ge 0.651 \text{ [7]} \qquad (6)$$

$$\rho = \begin{cases} \frac{0.772}{\bar{\lambda}_p}\phi(\alpha) - \frac{0.059}{\bar{\lambda}_p^2}\phi(\alpha)^2 + 0.01\alpha\bar{\lambda}_p^2 & 1 \le \alpha \le 3 \\ \frac{0.907}{\bar{\lambda}_p} - \frac{0.08\ 1}{\bar{\lambda}_p^2} + 0.03\bar{\lambda}_p^2 & \alpha > 3 \end{cases} \quad [8] \tag{7}$$

$$\phi(\alpha) = \frac{30.5+10.2\alpha-1.7\alpha^2}{39} \text{ with } 1 \le \alpha \le 3 \text{ [8]} \tag{8}$$

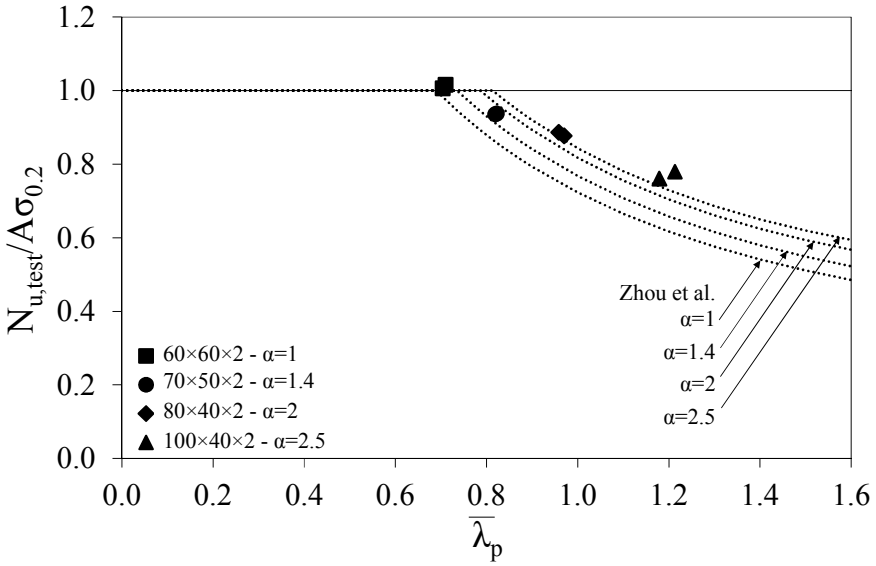

Fig. 16 Assessment of the reduction factor for Zhou et al. approach [8] for internal compressed elements

The predicted cross-section capacities $N_{u,pred}$ by these three design approaches and key statistical values concerning mean predictions and coefficient of variation (COV) relative to the test results are given in Table 10. As shown in Fig. 15, EN 1993-1-4 [1] is the lowest effective width curve and underestimates the test results, while Gardner and Theofanous [7] revised equation is more accurate. Overall, Zhou et al. [8] proposed curves provide a better approximation to the test results as observed in Fig. 16 and Table 10 with the lowest mean and coefficient of variation (COV).

Table 10. Comparison of predicted resistances by different approaches [1,7,8] for the stub columns

Specimen	Comparison		
	$N_{u,test}/N_{u,pred}$ [1]	$N_{u,test}/N_{u,pred}$ [7]	$N_{u,test}/N_{u,pred}$ [8]
60×60×2-SC1	1.189	1.084	1.042
60×60×2-SC2	1.172	1.067	1.025
70×50×2-SC1	1.017	1.083	1.015
70×50×2-SC2	1.020	1.089	1.021
80×40×2-SC1	1.119	1.076	1.033
80×40×2-SC2	1.122	1.079	1.030
100×40×2-SC1	1.086	1.052	1.013
100×40×2-SC2	1.086	1.052	1.013
Mean	1.123	1.065	1.030
COV	0.033	0.019	0.015

3.2.2 Elements in bending

The Class 3 slenderness limits for elements in bending specified in EN 1993-1-4 [1] and proposed by Gardner and Theofanous [7], together with the bending test results, are assessed in Fig. 17, where the test ultimate bending capacity $M_{u,test}$ has been normalised by the product of the elastic section modulus W_{el} and the 0.2% proof stress $\sigma_{0.2}$ and plotted against the slenderness parameter c/tε of the most slender constituent element in the cross-section controlling the local buckling response. Note that Fig. 17 includes the results corresponding to the specimen 100×40×2-4P tested about major axis, of which the element in bending (web) controlled the local buckling response; hence, exhibiting higher relevant slenderness $\overline{\lambda}_p$ than the uniformly compressed flange, see Table 9. From Fig. 17, it may be concluded that EN 1993-1-4 [1] slenderness limit of 74.8 is appropriate for ferritic stainless steel while no conclusions can be drawn for the proposed limit of 90 by Gardner and Theofanous [7].

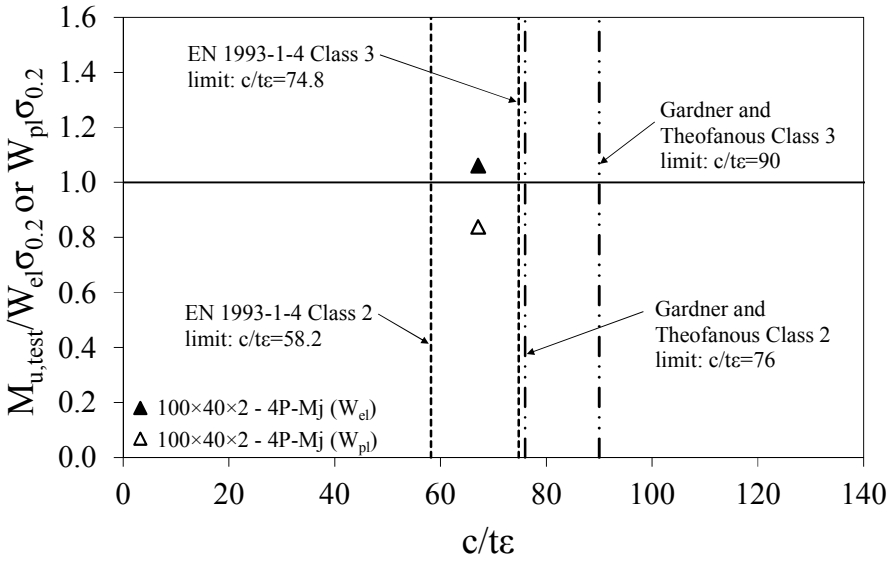

Fig. 17 Assessment of Class 3 and 2 limits for internal elements in bending (bending test results)

3.3 Assessment of Class 2 and 1 slenderness limits

3.3.1 Elements in compression

In Fig. 18, the experimental ultimate bending moment $M_{u,test}$ is normalized by the product of the plastic section modulus W_{pl} and the 0.2% proof stress $\sigma_{0.2}$ and plotted against the slenderness parameter c/tε of the most slender constituent element in the cross-section to assess the Class 2 slenderness limit for internal elements in compression specified in EN 1993-1-4 [1] and the proposed by Gardner and Theofanous [7]. This relevant response is also given in Table 9. From Fig. 18, it might be concluded that the current EN 1993-1-4 [1] Class 2 limit of 26.7 is applicable to ferritic stainless steel, but conservative, while the revised slenderness value of 35 proposed by Gardner and Theofanous [7] is more appropriate.

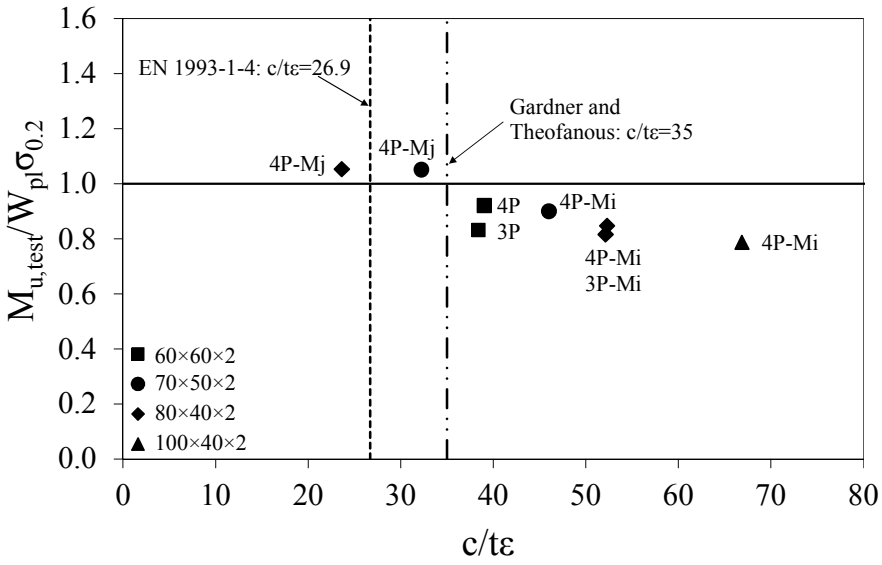

Fig. 18 Assessment of Class 2 limit for internal elements in compression (bending test results)

The rotation capacity of the bending test results reported in Table 8 is plotted against the flange slenderness in Fig. 19 to assess the Class 1 limit. Given the fact that there is no codified deformation capacity requirement for Class 1 stainless steel sections, the rotation capacity requirement of R=3 [30] for carbon steel is adopted herein, as has been assumed in existing investigations [5,26,27]. Even though the European standard for stainless steel does not allow plastic design, a Class 1 limit of 25.7 is given in EN 1993-1-4 [1]. This limit as well as Gardner and Theofanous [7] proposed value of 33 appear unsafe in Fig. 19 under the assumption that this rotation capacity requirement of R=3 is appropriate for stainless steel. Previous studies reported the influence of the material response on the rotation capacity R for various stainless steels [6, 26] which are believed to significantly reduce the ductility demands on stainless steel structures for plastic design, particularly the gradual yielding and considerable strain hardening. To date, there is neither enough available experimental data nor research on stainless steel regarding plastic design to conduct an accurate assessment for the Class 1 slenderness limit.

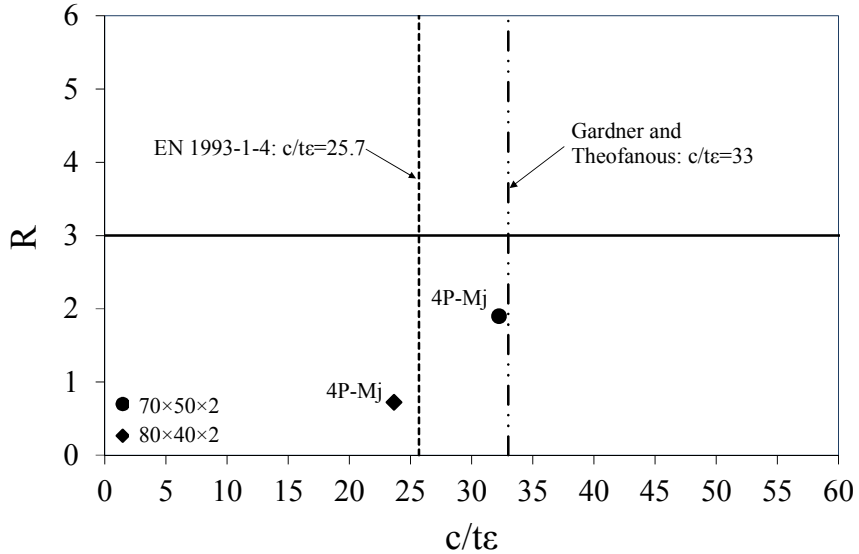

Fig. 19 Assessment of Class 1 limit for internal elements in compression (bending test results)

3.3.2 Elements in bending

The assessment of the Class 2 limit for internal elements in bending is shown in Fig. 17 together with the assessment of the Class 3 limit. For this case, the experimental ultimate bending moment $M_{u,test}$ is normalized by the product of the plastic section modulus W_{pl} and the 0.2% proof stress $\sigma_{0.2}$ (plastic moment capacity M_{pl}) and plotted against the slenderness parameter $c/t\varepsilon$ of the most slender constituent element subjected to bending in the cross-section and controlling the local buckling response, see Table 9. In Fig. 20 it is observed that the slenderness limit of 76 proposed by Gardner and Theofanous [7] is too optimistic, and the EN 1993-1-4 [1] value of 58.2 should be adopted for the design of ferritic stainless steel elements in bending.

4. Conclusions

An experimental investigation on the structural performance of cold-formed SHS and RHS structural elements on grade 1.4003 (similar to 3Cr12) ferritic stainless steel has been described in detail in the present paper. Tests were undertaken on 4 section geometries with different aspect ratios $\alpha=h/b$ ranging from 1 to 2.5 and featuring slender elements. A total of 16 tensile coupon tests, including flat parts and corners, 8 stub column tests, 2 3-point bending tests and 7 4-point bending tests about major and minor axis have been presented. The obtained test data were used to assess the applicability of the slenderness limits and effective width formulae of the current European specification for stainless steel, EN 1993-1-4 [1], those proposed by Gardner and Theofanous [7] and the design approach proposed by Zhou et al. [8], which accounts for the benefits of element interaction effects, to ferritic stainless steel. The assessment covered internal elements in compression (Class 1 to 4 and effective width method) and internal elements in bending (Class 2 and 3).

The results showed that the Class 3 slenderness limit and effective width equation for elements in compression given in EN 1993-1-4 [1] are applicable to ferritic stainless steel, though those proposed by Gardner and Theofanous [7] are more appropriate and this is the recommended approach for cross-section classification of slender elements. The proposed Class 3 limit by Zhou et al. [8] for aspect ratios of 1 (SHS) is also well suited for ferritic stainless steels but for aspect ratios >1 (RHS) the amount of tested sections, of which the achieved loads were consistent with the basis of this design method, is not representative to validate the applicability of this design approach to ferritic stainless steel sections and further research is essential to study the effects of element interaction in such sections. On the other hand, the cross-section resistance predicted by Zhou et al. [8] design method, using the reduction factor ρ as a function of the aspect ratio, more closely matched the test data in comparison with EN 1993-1-4 [1] and Gardner and Theofanous [8] approaches. Regarding the assessment of elements in bending, it was observed that the current Class 3 slenderness limit given in EN 1993-1-4 [1] is safe for application to ferritic stainless steel while no conclusion could be drawn for the Gardner and Theofanous [7] slenderness limiting value. The results also showed the adequacy of the Class 2 slenderness limits given in EN 1993-1-4 [1] for both internal elements in compression and bending, though the proposed slenderness values by Garner and Theofanous [7] for the formers reflect better the cross-sectional behaviour. For internal elements in bending, however, the proposed Class 2 limit by Gardner and Theofanous [7] was observed to be unsafe for application to ferritic stainless steels and the value given in EN 1993-1-4 [1] is therefore recommended. The necessity to conduct further research on plastic design was also highlighted to derive appropriate ductility demands and Class 1 slenderness limiting values for application to ferritic stainless steels.

Acknowledgements
The research leading to these results has received funding from Ministerio de Economía y Competitividad to the Project BIA 2012-36373 "Estudio del comportamiento de estructuras de acero inoxidable ferrítico". The authors are grateful to Acerinox Europa S.A.U for their contribution to the material experimental tests. We also want to thank Tomàs Garcia, Carlos Hurtado, Jorge Cabrerizo and Jordi Lafuente for their technical assistance and Toni Sastre for his contribution in the laboratory. The first and second authors would like to acknowledge the financial support provided by the Secretaria d'Universitats i de Recerca del Departament d'Economia i Coneixement de la Generalitat de Catalunya i del Fons Social Europeu to their FI-DGR 2012 and FI-DGR 2014 grants, respectively.

References
[1] EN 1993-1-4. Eurocode 3: Design of steel structures – Part 1 – 4: General rules – Supplementary rules for stainless steels. Brussels: European Committee for Standardization (CEN); 2006.

[2] Cashell KA, Baddoo NR. Ferritic stainless steels in structural applications. Thin-Walled Structures 2014;83:169-181.

[3] Bredenkamp PJ, van den Berg GJ. The strength of stainless steel built-up I-section columns. Journal of Constructional Steel Research 1995;34:131-144.

[4] Stangenberg H. Work package 6: Ferritic stainless steel. Report to the ECSC Project - Development of the use of stainless steel in construction. Contract no. 7210 SA/ 842. Germany: Studiengesellschaft Stanhlanwendung; 2000.

[5] Afshan S, Gardner L. Experimental study of cold-formed ferritic stainless steel hollow sections. Journal of Structural Engineering (ASCE) 2013;139:717-728.

[6] Bock M, Gardner L and Real E. Material and local buckling response of ferritic stainless steel sections. Thin-Walled Structures 89, 2015, 131-141.

[7] Gardner L, Theofanous M. Discrete and continuous treatment of local buckling in stainless steel elements. Journal of Constructional Steel Research 2008;64:1207-16.

[8] Zhou F, Chen Y. and Young B. Cold-formed high strength stainless steel cross-sections in compression considering interaction effects of constituent plate elements. Journal of Constructional Steel Research 2013;80:32-41.

[9] Cruise RB, Gardner L. Strength enhancements induced during cold forming of stainless steel sections. Journal of Constructional Steel Research 2008;64:1310-6.

[10] Ashraf M, Gardner L, Nethercot D. Strength enhancement of the corner regions of stainless steel cross-sections. Journal of Constructional Steel Research 2005;61:37-52.

[11] Rasmussen KJR, Hancock GJ. Design of cold-formed stainless steel tubular members. I: Columns. Journal of Structural Engineering (ASCE) 1993;119:2349–2367.

[12] Cruise RB, Gardner L. Residual stress analysis of structural stainless steel sections. Journal of Constructional Steel Research 2008;64:352-66.

[13] Jandera M, Gardner L, Machacek J. Residual stresses in cold-rolled stainless steel hollow sections. Journal of Constructional Steel Research 2008;64:1255-63.

[14] Huang Y, Young B. Material properties of cold-formed lean duplex stainless steel sections. Thin-Walled Structures 2012;54:72–81.

[15] EN ISO6892-1. Eurocode 3: Metallic materials – tensile testing – Part1: Method of test at room temperature. Brussels: European Committee for Standardization (CEN); 2006.

[16] Ramberg W, Osgood WR. Description of stress–strain curves by three parameters. Technical note No 902, Washington DC: National advisory committee for aeronautics; 1943.

[17] Rasmussen KJR. Full-range stress-strain curves for stainless steel alloys. Journal of Constructional Steel Research 2003;59:47-61.

[18] Mirambell E, Real E. On the calculation of deflections in structural stainless steel beams: an experimental and numerical investigation. Journal of Constructional Steel Research 2000;54:109-33.

[19] Gardner L, Nethercot DA. Experiments on stainless steel hollow sections, Part – 1: Material and cross-sectional behaviour. Journal of Constructional Steel Research 2004;60:1291-318.

[20] Galambos TV. Guide to stability design criteria for metal structures. 5th ed. New York: J. Wiley & Sons; 1998.

[21] Compression tests of stainless steel tubular columns. Investigation report S770. Sydney: Centre for Advanced Structural Engineering, University of Sydney; 1990.

[22] EN 1993-1-3. Eurocode 3: Design of steel structures – Part 1 – 3: General rules – Supplementary rules for cold-formed members and sheeting. Brussels: European Committee for Standardization (CEN); 2006.

[23] Rasmussen KJR, Hancock GJ. Design of cold-formed stainless steel tubular members II: Beams. Journal of Structural Engineering (ASCE) 1993;119:2368-86.

[24] EN 1993-1-1. Eurocode 3: Design of steel structures – Part 1 – 1: General rules and rules for buildings. Brussels: European Committee for Standardization (CEN); 2005.

[25] Theofanous M, Gardner L. Testing and numerical modelling of lean duplex stainless steel hollow section columns. Engineering Structures 2009;31:3047-58.

[26] Theofanous M, Gardner L. Experimental and numerical studies of lean duplex stainless steel beams. Journal of Constructional Steel Research 2010;66:816-825.

[27] Saliba N, Gardner L. Cross-section stability of lean duplex stainless steel welded I-sections. Journal of Constructional Steel Research 2013;80:1-14.

[28] EN 1993-1-5. Eurocode 3: Design of steel structures – Part 1 – 5: Plated structural elements. Brussels: European Committee for Standardization (CEN); 2006.

[29] Gardner L, Saari N, Wang F. Comparative experimental study of hot-rolled and cold-formed rectangular hollow sections. Thin-Walled Structures 2010;48:495-507.

[30] Sedlacek G, Feldmann M. The b/t-ratios controlling the applicability of analysis models in Eurocode 3, Part 1.1. Background Document 5.09 for chapter 5 of Eurocode 3, Part 1.1. Germany: Aachen; 1995.